MOUSE ORGANOID CULTURE IS A SUITABLE MODEL TO STUDY ESOPHAGEAL ION TRANSPORT MECHANISMS

Marietta Margaréta Korsós,[1] *Tamás Bellák,*[2,3] *Eszter Becskeházi,*[1] *Eleonóra Gál,*[1] *Zoltán Veréb,*[4] *Péter Hegyi,*[5,6,7] *Viktória Venglovecz*[1]

[1]Department of Pharmacology and Pharmacotherapy, University of Szeged, Szeged, Hungary
[2]Department of Anatomy, Histology and Embryology, University of Szeged, Szeged, Hungary
[3]BioTalentum Ltd., Gödöllő, Hungary
[4]Regenerative Medicine and Cellular Pharmacology Research Laboratory, Department of Dermatology and Allergology, University of Szeged, Szeged, Hungary
[5]First Department of Medicine, University of Szeged, Szeged, Hungary
[6]Institute for Translational Medicine, Medical School, Szentágothai Research Centre, University of Pécs, Pécs, Hungary
[7]Division of Gastroenterology, First Department of Medicine, Medical School, University of Pécs, Pécs, Hungary

Running title: Ion transporters of esophageal organoids

Corresponding author:

Viktória Venglovecz, Ph.D.
Department of Pharmacology and Pharmacotherapy
University of Szeged
Szeged
HUNGARY
Telephone: +36 62 545 677
Fax: +36 62 545 680
Email: venglovecz.viktoria@med.u-szeged.hu

Downloaded from journals.physiology.org/journal/ajpcell at Univ of Szeged (160.114.150.232) on September 16, 2021.

Downloaded from journals.physiology.org/journal/ajpcell at Univ of Szeged (160.114.150.232) on September 16, 2021.

ABSTRACT

Altered esophageal ion transport mechanisms play a key role in inflammatory and cancerous diseases of the esophagus, but epithelial ion processes have been less studied in the esophagus because of the lack of a suitable experimental model. In this study, we generated 3D esophageal organoids (EOs) from two different mouse strains and characterized the ion transport processes of the EOs. EOs form a cell-filled structure with a diameter of 250–300 μm and generated from epithelial stem cells as shown by FACS analysis. Using conventional PCR and immunostaining, the presence of Slc26a6 Cl^-/HCO_3^- anion exchanger (AE), Na^+/H^+ exchanger (NHE), Na^+/HCO_3^- cotransporter (NBC), cystic fibrosis transmembrane conductance regulator (CFTR) and anoctamin 1 Cl^- channels were detected in EOs. Microfluorimetric techniques revealed high NHE, AE, and NBC activities, whereas that of CFTR was relatively low. In addition, inhibition of CFTR led to functional interactions between the major acid–base transporters and CFTR. We conclude that EOs provide a relevant and suitable model system for studying the ion transport mechanisms of esophageal epithelial cells, and they can be also used as preclinical tools to assess the effectiveness of novel therapeutic compounds in esophageal diseases associated with altered ion transport processes.

Keywords: esophagus, ion transport, CFTR

Downloaded from journals.physiology.org/journal/ajpcell at Univ of Szeged (160.114.150.232) on September 16, 2021.

INTRODUCTION

Research in recent years has increasingly highlighted the importance of ion transport processes in inflammatory and cancerous diseases of the esophagus, as indicated by numerous clinical studies (1, 2). These studies revealed altered expression of individual acid–base transporters in Barrett's esophagus, squamous cell carcinoma, and adenocarcinoma. Conversely, the activity of these ion transporters has been less studied mainly because of the lack of a suitable experimental model. Currently, a number of esophageal cell lines ranging from normal cells to esophageal adenocarcinoma are available. Although cell lines are easy to maintain, they have also limitations. Some cell lines are genetically modified to preserve their proliferation or derived from pre-existing cancerous tissue, making them unsuitable for studying physiological processes. In addition, because of their genetic instability, cells can spontaneously differentiate into other cell types. The Ussing chamber is an old but commonly used apparatus for studying esophageal permeability, and it is also suitable for investigating transepithelial ion transport processes. However, application of this technique is often limited by the condition, permeability, and short life span of the tissue, as well as reproducibility.

Organoids are three dimensional cell culture systems derived from progenitor or stem cells that provide a near physiological *in vitro* model for studying epithelial function. The discovery of organoids has greatly contributed to improved understanding of the ion transport processes of individual organs such as the pancreas, colon, and airways (3-5). Esophageal organoids (EOs) were first derived from mouse esophageal tissue by DeWard et al. (6). The basal layer of the esophageal mucosa consists of a subpopulation of undifferentiated stem cells with self-renewal ability and high proliferative capacity. After proliferation, cells migrate toward the lumen while undergoing differentiation and replace the suprabasal cells (7). Under appropriate culture conditions, organoids grown from stem cells develop a similar

Downloaded from journals.physiology.org/journal/ajpcell at Univ of Szeged (160.114.150.232) on September 16, 2021.

structure as the organ of origin including the presence of several cell layers, but the difference is that the outermost layer is composed of basal undifferentiated cells and the internal cell mass is formed by differentiated keratinocytes (6).

Although EOs provide a suitable model for performing functional assays, the presence and activity of ion transporters have not been investigated using EOs. In this study, we characterized the activity and presence of ion transporters in mouse EOs for the first time. We illustrated that mouse EOs express functionally active Na^+/H^+ exchanger (NHE), Na^+/HCO_3^- cotransporter (NBC), Cl^-/HCO_3^- anion exchanger (AE), and cystic fibrosis transmembrane conductance regulator (CFTR) Cl^- channels. Our results provide insights into the ion transport defects related to certain esophageal diseases and highlight a relevant experimental model system for assessing the effects of drug molecules on esophageal ion transporters.

Downloaded from journals.physiology.org/journal/ajpcell at Univ of Szeged (160.114.150.232) on September 16, 2021.

Downloaded from journals.physiology.org/journal/ajpcell at Univ of Szeged (160.114.150.232) on September 16, 2021.

MATERIALS AND METHODS

Mice

Mice on the C57BL/6 and CD-1 backgrounds were bred and housed in standard plastic cages under a 12-h:12-h light-dark cycle at room temperature (23 ± 1°C), and they were given free access to standard laboratory chow and drinking solutions. Animal experiments were conducted in accordance with the Guide for the Care and Use of Laboratory Animals (US Department of Health and Human Services) and approved by the local Ethical Board of the University of Szeged.

Solutions and chemicals

General laboratory chemicals were obtained from Sigma-Aldrich (Budapest, Hungary). 2,7-Bis-(2-carboxyethyl)-5(6)-carboxyfluorescein acetoxymethyl ester (BCECF-AM) and N-(ethoxycarbonylmethyl)-6-methoxyquinolinium bromide (MQAE) were purchased from Molecular Probes Inc. (Eugene, OR, USA). BCECF-AM (2 μmol/L) and MQAE (5 μM) were prepared in dimethyl sulfoxide (DMSO) and stored at −20°C. 4-Isopropyl-3-methylsulfonylbenzoyl-guanidin methanesulfonate (HOE-642) was provided by Sanofi Aventis (Frankfurt, Germany) and dissolved in DMSO. Nigericin (10 mM) was prepared in ethanol and stored at −20°C. Forskolin was obtained from Tocris (Bristol, UK) and stored as a 250-mM stock solution in DMSO. The compositions of the solutions are presented in Table 1. Standard HEPES-buffered solutions were gassed with 100% O_2, and their pH was adjusted to 7.4 with NaOH. Standard HCO_3^-/CO_2-buffered solutions were gassed with 95% O_2/5% CO_2 to adjust their pH to 7.4. All experiments were performed at 37°C.

Isolation of esophageal epithelial cells (EECs)

After removal and longitudinal opening of the esophagus, the tissue was placed into dispase solution (2 U/mL) and incubated at 37°C for 40 min. Then, the mucosa was peeled from the submucosa using forceps, and the mucosa was incubated at 37°C in 1× trypsin–EDTA

Downloaded from journals.physiology.org/journal/ajpcell at Univ of Szeged (160.114.150.232) on September 16, 2021.

solution for 15 min, during which time the tissue was vortexed in every 2 min. To inactivate trypsin, the trypsin–EDTA solution (with floating cells) was pipetted into soybean trypsin inhibitor (STI) solution. The STI solution with the undigested tissue pieces was filter through a 40-μm cell strainer. Cells were then centrifuged for 10 min at 2000 rpm, and the cell pellet was resuspended in 300 μl of complete organoid culture medium.

Generation of EOs

The required volume of the cell suspension (7500 cells/well on a 24-well tissue culture plate) was mixed with Matrigel® extracellular matrix at a 40:60 ratio and portioned in the wells, followed by incubation at 37°C for 15 min to allow solidification of the gel. Complete organoid culture medium was added to cover the Matrigel® and incubated at 37°C. After 3–4 days, organoid formation was visible. They reach their maximum size on day 8–12. The growth medium consisted of Advanced Dulbecco's modified Eagle's medium/F12, 1× N2 and 1× B27 Supplements, 1× Glutamax (Gibco), 10 mM HEPES (Biosera), 2% penicillin/streptomycin (Gibco), 1 mM N-acetyl-L-cysteine (Sigma), 100 ng/mL R-spondin 1, 100 ng/mL Noggin (both from Peprotech), 50 ng/mL mouse epidermal growth factor (R&D), 10 μM Y27632 ROCK-kinase inhibitor (ChemCruz), and 5 % WNT3A conditioned medium. Wnt3A conditioned medium was prepared by collecting the supernatant from L-Wnt3A cells (ATCC CRL-2647) according to the manufacturer's protocol.

Flow cytometry

The expression of leucine-rich repeat-containing G-protein coupled receptor 5 (LGR5) and cytokeratin 14 (CK14) was measured by flow cytometry on a FACSCalibur flow cytometer (BD Biosciences Immunocytometry Systems, Franklin Lakes, NJ, USA) after staining the cells on ice for 30 min with LGR5-PE (Origene, TA400001) and CK14-FITC (Novusbio, NBP2-47720F) fluorochrome-conjugated antibodies and their matching isotype controls (PE Mouse IgG1, κ Isotype Ctrl Antibody #400111 and FITC Mouse IgG3, κ Isotype Ctrl

Downloaded from journals.physiology.org/journal/ajpcell at Univ of Szeged (160.114.150.232) on September 16, 2021.

158 Antibody #401317, both from Biolegend). The data were analyzed using Flowing Software
159 (Cell Imaging Core, Turku Center for Biotechnology, Finland), and the percentage of positive
160 cells was expressed as the mean ± SD.

161 **Immunofluorescence staining and histology**

162 Organoid cultures were fixed with 4% PFA in 0.1 mol/L phosphate buffer for 1 h at room
163 temperature and washed three times with PBS. The fixed samples were cryoprotected in 30%
164 sucrose solution (in PBS) containing 0.01% sodium azide at 4°C until embedding in Tissue-
165 Tek O.C.T. compound (Sakura). The 16-µm parallel sections were sectioned using a cryostat
166 (Leica CM 1850, Leica), mounted to gelatin-coated slides, and stored at −20°C until use.
167 After air-drying for 10 min, the sections were permeabilized with 0.1% Triton X-100 in PBS
168 and blocked for 1 h at 24°C with 3% BSA in PBS. The sections were then incubated with
169 primary antibodies (overnight, 4°C). On the next day, sections were washed in PBS three
170 times, and isotype-specific secondary antibodies were diluted in blocking buffer and applied
171 for 1 h at room temperature. The sections were washed three times with PBS and covered
172 using Vectashield® mounting medium containing DAPI (1.5 µg/mL, Vector Laboratories),
173 which labeled the nuclei of the cells. Immunoreactive sections were analyzed using a BX-41
174 epifluorescence microscope (Olympus) equipped with a DP-74 digital camera and CellSens
175 software (V1.18, Olympus) or using an Olympus Fv-10i-W compact confocal microscope
176 system (Olympus) with Fluoview Fv10i software (V2.1, Olympus). For hematoxylin and
177 eosin (HE) staining, sections were incubated with Mayer's Hematoxylin solution (Sigma) for
178 5 min. Sections were washed with tap water and incubated into distilled water twice for 3 min
179 each. Sections were then incubated in 1% eosin solution in distilled water (Sigma) for 2 min.
180 Stained sections were dehydrating through 96 and 100% alcohol, cleared in xylene, and
181 mounted in DPX (Sigma). Microphotographs were taken using a DP-74 digital camera using a
182 light microscope (BX-41) and CellSens software (V1.18). All images were further processed

Downloaded from journals.physiology.org/journal/ajpcell at Univ of Szeged (160.114.150.232) on September 16, 2021.

using the GNU Image Manipulation Program (GIMP 2.10.0) and NIH ImageJ analysis software (imagej.nih.gov/ij). Details of the primary and secondary antibodies are presented in Table 2.

Gene expression analysis using RT-PCR

Total RNA was isolated from the organoids using a NucleoSpin RNA Kit (Macherey–Nagel, Düren, Germany). Two micrograms of RNA were reverse-transcribed using a High-Capacity cDNA Reverse Transcription Kit (Applied Biosystems, Foster City, CA, USA). PCR was performed using DreamTaq DNA polymerase in a final volume of 20 μL. All reactions were performed under the following conditions: 94°C for 5 min; 30 cycles of 94°C for 30 s, 60°C for 30 s, and 72°C for 1 min; and final elongation at 72°C for 10 min. The PCR products (10 μL) were separated by electrophoresis on a 2% agarose gel and visualized using an AlphaImager EC Gel Documentation System. As a positive control, kidney cDNA was used in the case of Slc9a1, Slc9a2, Slc26a6, Slc4a4, and CFTR, and pancreas cDNA was used in the case of Slc26a3 and anoctamine-1 (ANO-1). Primer sequences are presented in Table 3.

Measurement of the intracellular Cl^- concentration ($[Cl^-]_i$) and pH microfluorimetry

EOs were attached to a poly-L-lysine–coated cover slip (24 mm) forming the base of a perfusion chamber and mounted on the stage of an inverted fluorescence microscope linked to the Xcellence imaging system (Olympus). Organoids were then bathed with different solutions at 37°C at a perfusion rate of 5–6 mL/min. Then, 6–12 region of interests (ROIs) were examined in each experiments, and one measurement was obtained per second. $[Cl^-]_i$ was estimated using the fluorescent dye MQAE. Specifically, organoids were incubated with MQAE (5 μM) for 2–3 h at 37°C, and changes in $[Cl^-]_i$ were determined by exciting the cells at 340 nm with emitted light monitored at 380 nm. Fluorescence signals were normalized to the initial fluorescence intensity (F/F0) and expressed as relative fluorescence. To determine intracellular pH (pH_i), cells were loaded with the pH-sensitive fluorescent dye BCECF-AM (2

Downloaded from journals.physiology.org/journal/ajpcell at Univ of Szeged (160.114.150.232) on September 16, 2021.

μM, 30 min, 37°C) and excited at 490 and 440 nm. The 490/440 fluorescence emission ratio was measured at 535 nm. The calibration of the fluorescence emission ratio to pH_i was performed using the high-K^+/nigericin technique, as previously described (8, 9).

Measurement of the activity of the acid–base transporters

To estimate the activity of NHE and NBC, the NH_4Cl prepulse technique was used. Briefly, exposure of EOs to 20 mM NH_4Cl for 3 min induced an immediate rise in pH_i because of the rapid entry of lipophilic basic NH_3 into the cells. After the removal of NH_4Cl, pH_i rapidly decreased. This acidification is caused by the dissociation of intracellular NH_4^+ to H^+ and NH_3, followed by the diffusion of NH_3 from the cells. In standard HEPES-buffered solution, the initial rate of pH_i ($\Delta pH/\Delta t$) recovery from the acid load (over the first 60 s) reflects the activities of NHEs, whereas in HCO_3^-/CO_2-buffered solutions, the rate represents the activities of both NHE and NBC (10).

Two independent methods were used to estimate AE activity. Using the NH_4Cl prepulse technique, the initial rate of pH_i recovery from alkalosis in HCO_3^-/CO_2-buffered solutions was analyzed (10). Previous data indicated that under these conditions, the recovery over the first 30 s reflects the activity of AE (10). The Cl^- withdrawal technique was also applied, in which removal of Cl^- from the external solution causes immediate and reversible alkalization of the pH_i because of the reverse operation of AE under these conditions. Previous data illustrated that the initial rate of alkalization over the first 60 s reflects the activity of AE (11).

Statistical analysis

Results are expressed as the mean ± SD. Statistical analyses were performed using analysis of variance. $p \leq 0.05$ was accepted as significant.

Downloaded from journals.physiology.org/journal/ajpcell at Univ of Szeged (160.114.150.232) on September 16, 2021.

RESULTS

Characterization of EO cultures

Isolated EECs were plated in Matrigel supplemented with organoid culture medium at a final concentration of 40%. On the 3rd day after plating, organoid formation was observed, and therefore, we assessed organoid growth starting from day 3 (Fig. 1A). The size of the organoids increased steadily in the following days, peaking between days 7 and 9. Organoids between 50 and 150 μm in size were used for our experiments. HE staining of the organoids illustrated that cells are located in several layers inside the organoids, matching the structure of normal esophageal tissue (Fig. 1B). The inner cell mass consisted of differentiated cells that move from the periphery to the inside of the organoids during their maturation. In addition, the centers of some organoids were empty, or they contained keratinized materials produced by the cells. To verify that organoids are generated from stem cells, we used the stem cell marker LGR5. Immunofluorescence staining revealed strong LGR5 expression in both C57BL/6 and CD-1 organoids (Fig. 1C), and FACS analysis demonstrated that 42.70 ± 7.27% of the isolated C57BL/6 EECs and 46.46 ± 7.81% of the isolated CD-1 EECs were LGR5-positive (Fig. 2A and B). In the next step, we verified that the organoids were derived from single EECs. CK14 is a cytoplasmic keratin expressed in the basal SECs (12, 13). As presented on Fig. 1C, the outer cell layer of the organoids was CK14-positive, indicating that the organoids originate from the mucosa and display a morphologically similar structure as normal esophageal tissue. FACS analysis indicated that 45.29 ± 9.25% of the isolated C57BL/6 EECs and 55.32 ± 7.80% of the isolated CD-1 EECs were CK14-positive (Fig. 2A and B). Interestingly, there was a slight difference in the double-positive (LGR5 and CK14) fraction. The proportion of double-positive cells was higher in CD-1 mouse organoids (35.37 ± 1.24%) than in C57BL/6 mouse organoids (19.34 ± 2.03%, Fig. 2C).

Downloaded from journals.physiology.org/journal/ajpcell at Univ of Szeged (160.114.150.232) on September 16, 2021.

mRNA and protein expression of ion transporters in EOs

The mRNA expression of ion transporters was investigated using conventional RT-PCR. We revealed the presence of *Slc9A1* (NHE-1), *Slc9A2* (NHE-2), *Slc26a6* (PAT1), *CFTR*, *Scl4a4* (NBCe1B), and *ANO1* in both the C57BL/6 and CD-1 organoids (Fig. 3A). The presence of these transporters was also confirmed at the protein level using immunohistochemistry (Fig. 3B and C). By contrast, the *Slc26a3* (DRA) transporter could not be detected at either the mRNA or protein level. Because the CFTR Cl^- channel and Slc26a6 interact with each other in several secretory epithelia (14), we examined the colocalization of these two transporters on the organoids. CFTR and Slc26a6 exhibited diffuse staining throughout cells without special localization to the apical or basal membrane. Interestingly, Slc26a6 staining was more detectable in cells on the periphery, whereas in the case of CFTR, central cells also displayed positive staining.

Resting pH_i of EOs and determination of buffering capacity

To investigate the pH regulatory mechanisms of EO cultures, we initially determined the resting pH_i of the cells. EOs were exposed to standard HEPES solution (pH 7.4), followed by a 5-min exposure to a high-K^+/nigericin–HEPES solution at pH 7.2, 7.4, and 7.6 (Fig. 4A). The resting pH_i of the organoids was determined using the classical linear model (8, 9). The resting pH_i of C57BL/6 organoids was 7.61 ± 0.03, whereas that of CD-1 organoids was 7.58 ± 0.03. The total buffering capacity (β_{total}) of EOs was estimated using the NH_4^+ prepulse technique, as previously described (Fig. 4B) (10, 15). Briefly, organoids were exposed to various concentrations of NH_4Cl in nominally Na^+- and HCO_3^--free solutions, and β_{total} of the cells was calculated using the following equation: $\beta_{total} = \beta_i + \beta_{HCO3}^- = \beta_i + 2.3 \times [HCO_3^-]_i$, where β_i describes the ability of intrinsic cellular components to respond to buffer changes of pH_i (calculated by the Henderson–Hasselbach equation) and β_{HCO3}^- is the buffering capacity of the HCO_3^-/CO_2 system. The measured rates of pH_i change ($\Delta pH/\Delta t$) were converted to

Downloaded from journals.physiology.org/journal/ajpcell at Univ of Szeged (160.114.150.232) on September 16, 2021.

transmembrane base flux $J(B^-)$ using the following equation: $J(B^-) = \Delta pH/\Delta t \times \beta_{total}$. β_{total} at the initial pH_i was used to calculate $J(B^-)$. We denoted base influx as $J(B)$ and base efflux (secretion) as $-J(B^-)$.

Activity of NHE

NHE is an integral plasma membrane protein that mediates the electroneutral exchange of extracellular Na^+ and intracellular H^+, thereby playing an important role in the alkalization of cells. NHE activity was investigated by removing extracellular Na^+ from the external solution. As presented in Figure 5A, Na^+ removal induced a sharp decrease in pH_i, suggesting that EOs express functionally active NHE. There was no significant difference in the rate ($-J(B^-)$) and extent (ΔpH_{max}) of the pH_i decrease between the two mouse strains (Fig. 5B and C). The presence of NHE was also confirmed using the ammonium prepulse technique (Fig. 5D). Organoids were exposed to 20 mM NH_4Cl (3 min) in standard HEPES-buffered solution, which induced a high degree of intracellular alkalization because of the rapid influx of NH_3 into cells. After removing NH_4Cl from the bath, pH_i dramatically decreased and then returned to baseline. Under these conditions, recovery from acidosis reflects the activity of NHE. In the absence of Na^+, recovery from acidosis was negligible, indicating that in the absence of HCO_3^-, NHE is mainly responsible for the alkalization of cells (Fig. 5D and E). The NHE gene family contains several isoforms (NHE-1–9) with different functions and expression patterns (16). To identify the most active isoform on organoids, the NHE isoform specific inhibitor HOE-642 was used. This inhibitor blocks NHE-1 and NHE-2 isoforms in a concentration-dependent manner. At a concentration of 1 μM, only the NHE-1 isoform is inhibited, whereas 50 μM HOE-642 inhibits both isoforms (2, 17). We chose this inhibitor because our previous studies on human esophageal cell lines indicated that these two isoforms are responsible for the majority of NHE activity (2). Organoids were acid-loaded with 20 mM NH_4Cl followed by a 3-min incubation in Na^+-free HEPES solution. In the absence of Na^+,

Downloaded from journals.physiology.org/journal/ajpcell at Univ of Szeged (160.114.150.232) on September 16, 2021.

307 the NHE is blocked, and thus, pH_i is not regenerated. Upon the re-administration of
308 extracellular Na^+, NHE regained its function, and its activity could be estimated from the
309 initial rate of pH_i recovery over the first 60 s. As presented in Fig. 6A, 1 μM HOE-642
310 decreased pH_i recovery by 87.81 ± 1.17% in C57BL/6 organoids and 82.37 ± 7.32% in CD-1
311 organoids, whereas the administration of 50 μM HOE-642 resulted in further decreases (97.54
312 ± 0.52% in C57BL/6 organoids and 92.91 ± 3.76% in CD-1 organoids, Fig. 6B). These data
313 indicate that although NHE-1 has higher activity, NHE-2 is also active on organoids. The fact
314 that some activity remained even in the presence of 50 μM HOE-642 suggests the presence of
315 other Na^+-dependent acid-extruding mechanisms.

316 **Activity of NBC**

317 NBC is an electrogenic transporter that mainly localizes to the basolateral membrane in most
318 epithelia, in which it mediates the cotransport of Na^+ and HCO_3^- into cells. Inside cells,
319 HCO_3^- binds H^+ and causes intracellular alkalization. Therefore, in standard HCO_3^-/CO_2-
320 buffered external solution, both NHE and NBC fight against cellular acidosis. NBC activity
321 was investigated by the NH_4Cl prepulse technique (Fig. 7A). Administration of HCO_3^-/CO_2
322 rapidly and greatly decreased pH_i because of the quick diffusion of CO_2 into the cytoplasm.
323 Significant pH_i recovery was observed after acidification, suggesting the important role of
324 HCO_3^- efflux into EOs through NBC (Fig. 7A). After the NH_4Cl pulse, recovery from
325 alkalosis was more rapid than observed in the presence of standard HEPES-buffered solution,
326 indicating that in addition to NHE, NBC is also active in the presence of HCO_3^-. Removal of
327 Na^+ from the external solution almost completely abolished the recovery from acidosis. To
328 determine NBC activity, NHE function was blocked by the non-specific NHE inhibitor
329 amiloride, which was added 1 min before and during the re-administration of Na^+. As
330 presented in Fig. 7A and B, the recovery from acidosis was decreased by 61.88 ± 5.3% in
331 C57BL/6 organoids and 62.18 ± 7.3% in CD-1 organoids in the presence of amiloride,

Downloaded from journals.physiology.org/journal/ajpcell at Univ of Szeged (160.114.150.232) on September 16, 2021.

indicating that NHE is responsible for much of the recovery from acidosis, but there is also functionally active NBC on the cells. Interestingly, we found a significant difference in recovery following Na^+ deprivation between the C57BL/6 and CD-1 organoids, suggesting greater NBC activity in C57BL/6 mice.

Activity of the Cl^-/HCO_3^- exchanger

The HCO_3^- transporter family includes several transport proteins, of which Slc26 proteins functions as an electroneutral Cl^-/HCO_3^- exchanger. Among the Slc26 exchangers, the presence of Slc26a6 (PAT1) was detected at both the mRNA and protein level in the C57BL/6 and CD-1 organoids. Slc26a6 mediates Cl^- and HCO_3^- exchange with a $1Cl^-/2HCO_3^-$ stoichiometry. To determine whether this Cl^-/HCO_3^- exchanger is functionally active on the organoids, the Cl^- removal technique was used (Fig. 8A–C). In the presence of external Cl^-, Slc26a6 mediates the efflux of HCO_3^- and the uptake of Cl^-, therefore playing role in the acidification of cells. Removal of Cl^- from standard HCO_3^-/CO_2-buffered solution induced strong alkalization because of the reverse mode of the exchanger (Fig. 8A). By contrast, in the absence of HCO_3^-, Cl^- removal caused minimal, reversible alkalization (Fig. 8B). The presence of functionally active AE has been also confirmed by the NH_4Cl prepulse technique (Fig. 8D and E). We previously illustrated that in the presence of HCO_3^-, the initial rate of recovery (30 s) from alkalosis reflects the activity of Cl^-/HCO_3^- exchangers (11, 18). As presented in Fig. 8E, there was no significant difference in AE activity between the two mouse organoids.

Activity of CFTR

The CFTR Cl^- channel, which is present on most epithelial cells, mediates the efflux of Cl^- from cells. The presence of this ion channel has been detected at both the mRNA and protein level in organoids; therefore, we also investigated its activity using the Cl^- sensitive fluorescent dye MQAE and CFTR activator forskolin. As presented in Fig. 9A and B, the

Downloaded from journals.physiology.org/journal/ajpcell at Univ of Szeged (160.114.150.232) on September 16, 2021.

administration of 10 μM forskolin caused a small increase in initial rate of Cl^- efflux (19.61 ± 4.52% in C57BL/6 organoids and 21.83 ± 9.72% in CD-1 organoids), and Cl^- loss reached steady state after approximately 10 min. The effect of 5 μM forskolin was negligible. To investigate whether there is a functional relationship between CFTR and the acid–base transporters, the activity of the transporters was examined in the presence of the CFTR inhibitor CFTRinh-172 (10 μM, Fig. 9C–E). Using the NH_4Cl prepulse technique, we found that the activity of AE was significantly decreased by CFTR inhibition (18.60 ± 3.34% in C57BL/6 organoids and 35.71 ± 11.77% in CD-1 organoids, Fig. 9D), whereas recovery from acidosis was only inhibited in C57BL/6 organoids (Fig. 9E).

CONCLUSION

The present study is the first to describe and functionally characterize the most common ion transport processes on EOs using two frequently used laboratory mouse strains (C57BL/6 and CD-1). Regulation of pH_i in epithelial cells is crucial, as most biological processes are affected by changes in pH. Ion transporters are involved in the regulation of pH_i and extracellular pH. Specifically, the transporters are polarized on epithelial cells, ensuring the unidirectional movement of substances. Esophageal ion transport processes were most intensively studied in the 1990s, mostly using primary tissue. These studies investigated the basic acid–base transporters and characterized the effect of acid and bile on the function of these transporters (1). Although extremely important information was obtained from these investigations, most of the findings are obsolete, and the primary tissues used in these studies did not permit the specific investigation of a given transporter. The development of organoid cultures was a significant breakthrough in the examination of individual organs and tissues. Their biggest advantages include their easy maintenance, suitability for longer studies, and

Downloaded from journals.physiology.org/journal/ajpcell at Univ of Szeged (160.114.150.232) on September 16, 2021.

recapitulation of physiological conditions. In addition, organoids can be frozen and passaged, allowing the function of different transporters to be compared even on the same genetic background.

To investigate the ion transport mechanisms of EOs, we initially determined the resting pH and total buffering capacity of the cells. We found that the starting pH of the organoids was nearly 7.6 in CD-1 organoids and slightly higher than 7.6 in C57BL/6 organoids. This unusually high initial pH has also been detected in human and rabbit esophageal cells (19, 20).The cause of the high resting pH_i is not fully known. Presumably, this finding can be explained by the excessive activity of the alkalizing transporters that act against acidosis. Our results demonstrated the presence of a Na^+-dependent H^+ efflux mechanism on EOs, probably NHE, which was functionally active. The presence of NHE-1 on rat and rabbit EECs was previously demonstrated (21). By contrast, NHE-1 and NHE-2 expression is extremely low in normal human esophagus but strong in Barrett's and esophageal cancer (2, 22, 23). HOE-642 largely inhibited NHE function, suggesting that more than 90% of functionally active NHEs in EOs are NHE-1 and NHE-2. Concerning the residual activity, other NHE isoforms or a proton pump is presumably responsible. One possible candidate is NHE3, which was previously detected on human esophageal cells, in which it participate in the formation of dilated intercellular spaces, and the expression of this isoform increases with the severity of GERD (24, 25). Immunolocalization of NHE-1 and NHE-2 demonstrated that NHE-1 expression was mostly observed in the periphery, whereas NHE-2 staining was more pronounced in the inner cell layers. The different localization of NHE-1 and NHE-2 can be explained by the fact that organoids are composed of different types of cells. The outermost cell layer of the organoids consists of basal cells, whereas the inner cell layers are composed of differentiated keratinocytes. This indicates that NHE-1 is mainly expressed in basal cells, whereas NHE-2 is expressed in keratinocytes. Our finding that NHE-1 is mainly located in

Downloaded from journals.physiology.org/journal/ajpcell at Univ of Szeged (160.114.150.232) on September 16, 2021.

basal cells is consistent with the observation that NHE-1 expression is very extremely in human SECs (2, 22, 23).

NBC is another transporter that can protect cells from acidosis. We revealed the presence of NBC in EOs, and it plays an important role in pH_i regulation. CO_2-induced acidosis was almost completely reversed, which can be explained by the influx of HCO_3^- through NBC. Furthermore, we found a significant difference in recovery from acidosis in the presence and absence of HCO_3^-, and fairly significant recovery was observed in the presence of amiloride. Taken together, these data strongly indicate that EOs express functionally active NBC. The presence of NBC has to date been identified in submucosal glands, in which it plays role in HCO_3^- secretion (26, 27). The presence of NBC has also been demonstrated in human EECs, and similarly as NHE, its expression is increased in Barrett's carcinoma (2). The role of NBC in SECs is not entirely clear, but presumably, it might play a central role in the regulation of pH_i and transcellular transport of HCO_3^-. Because NBC mediates HCO_3^- uptake, its present also presupposes the presence of AE on these cells. Using a microfluorimetric technique, we detected a Cl^--dependent HCO_3^- efflux mechanism on EOs. Removal of Cl^- from the external solution in the presence of HCO_3^- induced strong alkalosis via the reverse mode of the Cl^-/HCO_3^- exchanger. In addition, the presence of HCO_3^- significantly increased the rate of recovery from alkalosis. Previous studies by our laboratory demonstrated that recovery from alkalosis in the presence of HCO_3^- is the result of HCO_3^- efflux through the Cl^-/HCO_3^- exchanger (11, 18). Among the Cl^-/HCO_3^- exchangers, the presence of Na^+-dependent and Na^+-independent transporters was demonstrated on rabbit SECs (28). In addition, the presence of Slc26a6 was detected on SMGs, thereby mediating HCO_3^- secretion together with NBC and CFTR (26, 27). In EOs, strong Slc26a6 expression was found at both the mRNA and protein level, whereas Slc26a3 expression was weak and non-specific. The Slc26a6 transporter is primarily located on the apical membrane of secretory epithelial cells, in which

Downloaded from journals.physiology.org/journal/ajpcell at Univ of Szeged (160.114.150.232) on September 16, 2021.

it plays an essential role in HCO_3^- secretion (29). Because the esophageal epithelium is not a typical secretory epithelium, the presence of this transporter on EOs is unusual. In addition, Slc26a6 expression was more pronounced at the periphery, indicating that basal cells have some HCO_3^--secreting capacity. In many secretory epithelia, Slc26 AEs interact with the CFTR Cl^- channel in the regulation of HCO_3^- secretion (30, 31). To investigate the presence of CFTR and its coexpression with the Slc26a6 transporter, we investigated the colocalization of these transporters using immunostaining. As an interesting finding of our study, the CFTR Cl^- channel is expressed on EOs. Immunolocalization illustrated that both peripheral and central cells highly express CFTR. Costaining of CFTR and Slc26a6 revealed some colocalization, mainly in cells on the periphery, indicating that the two transporters interact with each other. To investigate the functional interaction between CFTR and Slc26a6, the microfluorimetric technique was used. The specific CFTR activator forskolin concentration-dependently increased the activity of CFTR, although the response to forskolin was relatively low even in the presence of supramaximal concentrations, indicating that CFTR channel activity is lower than usually observed for secretory epithelia, such as those in the pancreas or lungs (32). The presence of the CFTR inhibitor CFTRinh-172 decreased the rate of recovery from alkalosis in both C57BL/6 and CD-1 organoids, indicating that the channel interacts with the AE. Interestingly, we found that CFTR inhibition also significantly reduced recovery from acidosis in C57BL/6 organoids. Because both NBC and NHE are involved in recovery from acidosis in the presence of HCO_3^-, CFTR interacts with one of these transporters, but this type of interaction was not previously described. CFTR has been detected in the ductal cells of porcine submucosal glands, in which it localizes primarily to the apical membrane and plays an important role in ductal HCO_3^- secretion (26). It has also been detected in SECs, in which its presence is restricted to the basal cell layer (33). In SECs, CFTR mediates Cl^- transport together with the voltage-gated Cl^- channel ClC-2, which plays a pivotal role in

Downloaded from journals.physiology.org/journal/ajpcell at Univ of Szeged (160.114.150.232) on September 16, 2021.

protection against acid-induced injury, as demonstrated with the ClC-2 agonist lubiprostone (33). Because lubiprostone has been illustrated to activate CFTR (34, 35), the role of CFTR in this process has been postulated. The protective role of CFTR was also demonstrated in BE and esophageal cancer (36-40). These experiments demonstrated that CFTR plays a protective role against esophageal cancer, and overexpression of this channel is associated with good prognosis in squamous cell carcinoma. We also revealed the presence of the Ca^{2+}-activated Cl^- channel ANO1 or TMEM16A in EOs. One study examined the presence of ANO1 in the esophageal epithelium and indicated that its expression is increased in eosinophilic esophagitis and correlated with the severity of the disease. Furthermore, ANO1 has been reported to play central roles in the proliferation of basal zone hyperplasia via an IL-13–mediated pathway (41).

In this study, we uncovered for the first time the presence of the major epithelial ion transporters in EOs. We demonstrated that NHE, NBC, AE, and the CFTR Cl^- channel are active in EOs, and there was no significant difference in the expression and activity of NHE, AE, and CFTR between the two mouse strains. We can conclude that the EOs comprise a suitable experimental system to investigate ion transport processes, and therefore, they can be used to study the role of ion transporters in different esophageal diseases or test drug molecules that affect the function of ion transporters.

Downloaded from journals.physiology.org/journal/ajpcell at Univ of Szeged (160.114.150.232) on September 16, 2021.

FUNDING

This study was supported by the National Research, Development and Innovation Office (FK123982), the National Research, Development and Innovation Office, by the Ministry of Human Capacities (EFOP 3.6.2-16-2017-00006).

CONFLICTS OF INTEREST

The authors hereby declare that there are no conflicts of interests to disclose.

AUTHORS CONTRIBUTION STATEMENT

MMK performed PCR and microfluorimetric measurements and analysed the data. TB did the immunostainings. EB participated in the culturing and microfluorimetric measurements of organoids. EG and ZV carried out FACS experiments and analysis. PH contributed to the interpretation of the results. VV supervised the project and drafted the manuscript. All authors discussed the results and contributed to the final manuscript. All authors approved the final version of the manuscript, agreed to be accountable for all aspects of the work in ensuring that questions related to the accuracy or integrity of any part of the work are appropriately investigated and resolved; and all persons designated as authors qualify for authorship, and all those who qualify for authorship are listed.

Downloaded from journals.physiology.org/journal/ajpcell at Univ of Szeged (160.114.150.232) on September 16, 2021.

FIGURE LEGENDS

Fig. 1 Characterization of esophageal organoids (EOs). (A) Representative bright field images of EOs grown for 9 days from freshly isolated esophageal mucosa. Images were taken using an Olympus IX71 inverted microscope. The scale bar represents 100 μm. (**B**) Hematoxylin and eosin staining of EOs developed from C57BL/6 and CD-1 mouse esophageal tissue. The scale bar represents 100 μm (upper line) and 50 μm (bottom line), respectively. (**C**) Confocal images of EOs stained for leucine-rich repeat-containing G-protein coupled receptor 5 (LGR5, green), cytokeratin 14 (CK14, red), and DAPI (blue). The scale bar represents 100 μm (main photo) and 50 μm (inset photo), respectively.

Fig. 2 Flow cytometry analysis of leucine-rich repeat-containing G-protein coupled receptor 5 (LGR5) and cytokeratin 14 (CK14) expression. (A) Percentage of LGR5- and CK14-positive cells in the cell suspension of esophageal mucosa obtained from CD-1 and C57BL/6 mice. (**B**) Representative histograms of the FACS analysis with the respective isotype controls (gray color). (**C**) Representative dot plots present CK14 and LGR5 double-positive cells. n = 3

Fig. 3 Expression of ion transporters in esophageal organoids (EOs). (A) Mature EOs were collected 9 days after plating, and RNA was prepared from the organoids. Gene expression of ion transporters was investigated with traditional RT-PCR analysis. (**B**) Immunostaining of EOs for Slc9a1 (first line), Slc9a2 (second line), Slc26a3 (third line), Slc4a4 (fourth line), and ANO1 (fifth line). The scale bar represents 100 μm (main photo) and 50 μm (inset photo), respectively.

(**C**) Costaining of Slc26a6 (red) and CFTR (green). The scale bar represents 50 μm (upper line), 25 μm (middle line) and 10 μm (bottom line), for both mice strains.

Downloaded from journals.physiology.org/journal/ajpcell at Univ of Szeged (160.114.150.232) on September 16, 2021.

Fig. 4 Initial pH and buffering capacity of esophageal organoids. (A) Organoids were exposed to nigericin/high-K^+–HEPES solution at pH 7.2, 7.4, and 7.6. The resting intracellular pH (pH_i) was calculated from this three-point calibration using the classic linear model. (**B**) Organoids were exposed to various concentrations of NH_4Cl in nominally Na^+- and HCO_3^--free solutions, and the total buffering capacity (β_{total}) of the cells was calculated using the following equation: $\beta_{total} = \beta_i + \beta_{HCO3-} = \beta_i + 2.3 \times [HCO_3^-]_i$, where β_i refers to the ability of intrinsic cellular components to buffer changes of pH_i and β_{HCO3^-} is the buffering capacity of the HCO_3^-/CO_2 system. The black line shows the organoid response isolated from C57BL/6 mice, whereas the red line shows the organoid response isolated from CD-1 mice. n = 17-19

Fig. 5 Investigation of Na^+/H^+ exchanger (NHE) activity in esophageal organoids (EOs). (**A**) Removal of Na^+ from standard HEPES solution caused rapid intracellular acidosis in organoids isolated from C57BL/6 (black line) and CD-1 (red line) mice confirmed the presence of a Na^+-dependent H^+ efflux mechanism. Summary data for the maximal intracellular pH (pH_i) change (ΔpH_{max}) (**B**) and the calculated base flux ($J(B^-)$) (**C**) induced by Na^+ removal. (**D**) Recovery from acid load reflects the activity of NHE in standard HEPES-buffered solution. After the second NH_4Cl pulse, Na^+ was removed from the external solution to investigate the activity of NHE. (**E**) Summary bar chart presents the initial rate of pH_i recovery ($J(B^-)$) from an acid load. $J(B^-)$ was calculated from the dpH/dt obtained by linear regression analysis of pH_i measurements made over the first 60 s after Na^+ removal (one pH_i measurement was made per second). The buffering capacity at the initial pH_i was used for the calculation of $J(B^-)$ (see Methods). Data are presented as the mean ± SD. a: $p \leq 0.05$ vs. Control. n = 19-23

Fig. 6 Investigation of Na^+/H^+ exchanger (NHE) isoforms on esophageal organoids (EOs). (**A**) Representative intracellular pH (pH_i) curves (black line, C57BL/6; red line, CD-1)

Downloaded from journals.physiology.org/journal/ajpcell at Univ of Szeged (160.114.150.232) on September 16, 2021.

present the recovery from acidosis in the presence of 1 and 50 μM HOE-642. (**B**) Summary data of the calculated activities of the different NHE isoforms in the presence of the isoform-selective NHE inhibitor HOE-642. The rate of pH recovery ($J(B^-)$) was calculated from the $\Delta pH/\Delta t$ obtained via linear regression analysis of the pH_i measurement performed over the first 60 s of recovery from the lowest pH_i level (initial pH_i). The buffering capacity at the initial pH_i was used to calculate $J(B^-)$. Data are presented as the mean ± SD. a: $p \leq 0.05$ vs. Control. b: $p \leq 0.05$ vs. 1 μM HOE-642. n = 5–11

Fig. 7 Investigation of Na^+/HCO_3^- cotransporter (NBC) activity in esophageal organoids (EOs). (**A**) Representative intracellular pH (pH_i) curves (black line, C57BL/6; red line, CD-1) present the recovery from acidosis in the presence of 0.2 mM amiloride. (**B**) Summary data present the calculated activity of NBC in the presence of the Na^+/H^+ exchanger (NHE) inhibitor amiloride. The rate of acid recovery ($J(B^-)$) was calculated from the $\Delta pH/\Delta t$ obtained via linear regression analysis of the pH_i measurement performed over the first 60 s of recovery from the lowest pH_i (initial pH_i). The buffering capacity at the initial pH_i was used to calculate $J(B^-)$. Data are presented as the mean ± SD. a: $p \leq 0.05$ vs. Control. b: $p \leq 0.05$ vs. C57BL/6. n = 15–17

Fig. 8 Investigation of Cl^-/HCO_3^- exchanger activity in esophageal organoids.

Cl^-/HCO_3^- exchanger activity was investigated by the Cl^- removal technique in the presence (**A**) and absence (**B**) of HCO_3^-/CO_2 (black line, C57BL/6; red line, CD-1) (**C**) The rate of acid recovery $J(B^-)$ was calculated from the dpH/dt obtained via linear regression analysis of intracellular pH (pH_i) measurements performed over the first 60 s after exposure to the Cl^--free solution. The buffering capacity at the initial pH_i was used to calculate $J(B^-)$. n = 4-15 (**D**) The activity of the Cl^-/HCO_3^- exchanger was also measured using the alkali loading method and expressed as calculated $J(B^-)$, which was calculated from the dpH/dt obtained via linear regression analysis of pH_i measurements performed over the first 30 s of recovery from

Downloaded from journals.physiology.org/journal/ajpcell at Univ of Szeged (160.114.150.232) on September 16, 2021.

the highest pH_i level (initial pH_i) achieved in the presence of NH_4Cl. The buffering capacity at the start point pH_i was used for the calculation of $J(B^-)$. Data are presented as the mean ± SD. n = 25-37

Fig. 9 Investigation of cystic fibrosis transmembrane conductance regulator (CFTR) activity in esophageal organoids (EOs). (A) Representative intracellular pH (pH_i) curves (black line, C57BL/6; red line, CD-1) present the effect of forskolin on Cl^- efflux. **(B)** Summary data for the maximal fluorescence intensity changes. n = 19-22 (**C**) Representative pH_i curves present the recovery from acid and alkali loading in the presence of 10 μM CFTRinh-172. The rates of alkali recovery ($-J(B^-)$) (**D**) and acid recovery ($J(B^-)$) (**E**) were calculated from the $\Delta pH/\Delta t$ obtained via linear regression analysis of pH_i measurements performed over the first 30 and 60 s of recovery from the highest and lowest pH_i (initial pH_i), respectively. The buffering capacity at the initial pH_i was used to calculate $J(B^-)$ and $-J(B^-)$. Data are presented as the mean ± SD. a: $p \leq 0.05$ vs. Control. b: $p \leq 0.05$ vs. C57BL/6. n = 3–6

Table 1. Compositions of the solutions. Values are presented in mM.

Table 2. List of primary and secondary antibodies used in the study

Table 3. Primer sequences used in the study

Downloaded from journals.physiology.org/journal/ajpcell at Univ of Szeged (160.114.150.232) on September 16, 2021.

600

601

602

603

Downloaded from journals.physiology.org/journal/ajpcell at Univ of Szeged (160.114.150.232) on September 16, 2021.

REFERENCES

1. **Becskehazi E, Korsos MM, Eross B, Hegyi P, and Venglovecz V**. OEsophageal Ion Transport Mechanisms and Significance Under Pathological Conditions. *Front Physiol* 11: 855, 2020.

2. **Laczko D, Rosztoczy A, Birkas K, Katona M, Rakonczay Z, Jr., Tiszlavicz L, Roka R, Wittmann T, Hegyi P, and Venglovecz V**. Role of ion transporters in the bile acid-induced esophageal injury. *Am J Physiol Gastrointest Liver Physiol* 311: G16-31, 2016.

3. **de Jonge H.R. BMJC, Strubberg A.M., Liu J., Clarke L.L.** Organoids as a Model for Intestinal Ion Transport Physiology. In: *Ion Transport Across Epithelial Tissues and Disease*, edited by Hamilton K.L. DDCSpringer, Cham., 2020.

4. **Molnar R, Madacsy T, Varga A, Nemeth M, Katona X, Gorog M, Molnar B, Fanczal J, Rakonczay Z, Jr., Hegyi P, Pallagi P, and Maleth J**. Mouse pancreatic ductal organoid culture as a relevant model to study exocrine pancreatic ion secretion. *Lab Invest* 100: 84-97, 2020.

5. **Sachs N, Papaspyropoulos A, Zomer-van Ommen DD, Heo I, Bottinger L, Klay D, Weeber F, Huelsz-Prince G, Iakobachvili N, Amatngalim GD, de Ligt J, van Hoeck A, Proost N, Viveen MC, Lyubimova A, Teeven L, Derakhshan S, Korving J, Begthel H, Dekkers JF, Kumawat K, Ramos E, van Oosterhout MF, Offerhaus GJ, Wiener DJ, Olimpio EP, Dijkstra KK, Smit EF, van der Linden M, Jaksani S, van de Ven M, Jonkers J, Rios AC, Voest EE, van Moorsel CH, van der Ent CK, Cuppen E, van Oudenaarden A, Coenjaerts FE, Meyaard L, Bont LJ, Peters PJ, Tans SJ, van Zon JS, Boj SF, Vries RG, Beekman JM, and Clevers H**. Long-term expanding human airway organoids for disease modeling. *EMBO J* 38: 2019.

Downloaded from journals.physiology.org/journal/ajpcell at Univ of Szeged (160.114.150.232) on September 16, 2021.

6. **DeWard AD, Cramer J, and Lagasse E**. Cellular heterogeneity in the mouse esophagus implicates the presence of a nonquiescent epithelial stem cell population. *Cell Rep* 9: 701-711, 2014.

7. **Kalabis J, Oyama K, Okawa T, Nakagawa H, Michaylira CZ, Stairs DB, Figueiredo JL, Mahmood U, Diehl JA, Herlyn M, and Rustgi AK**. A subpopulation of mouse esophageal basal cells has properties of stem cells with the capacity for self-renewal and lineage specification. *J Clin Invest* 118: 3860-3869, 2008.

8. **Thomas JA, Buchsbaum RN, Zimniak A, and Racker E**. Intracellular pH measurements in Ehrlich ascites tumor cells utilizing spectroscopic probes generated in situ. *Biochemistry* 18: 2210-2218, 1979.

9. **Hegyi P, Rakonczay Z, Jr., Gray MA, and Argent BE**. Measurement of intracellular pH in pancreatic duct cells: a new method for calibrating the fluorescence data. *Pancreas* 28: 427-434, 2004.

10. **Hegyi P, Gray MA, and Argent BE**. Substance P inhibits bicarbonate secretion from guinea pig pancreatic ducts by modulating an anion exchanger. *American journal of physiology Cell physiology* 285: C268-276, 2003.

11. **Venglovecz V, Rakonczay Z, Jr., Ozsvari B, Takacs T, Lonovics J, Varro A, Gray MA, Argent BE, and Hegyi P**. Effects of bile acids on pancreatic ductal bicarbonate secretion in guinea pig. *Gut* 57: 1102-1112, 2008.

12. **Harnden P, and Southgate J**. Cytokeratin 14 as a marker of squamous differentiation in transitional cell carcinomas. *J Clin Pathol* 50: 1032-1033, 1997.

13. **Reis-Filho JS, Simpson PT, Martins A, Preto A, Gartner F, and Schmitt FC**. Distribution of p63, cytokeratins 5/6 and cytokeratin 14 in 51 normal and 400 neoplastic human tissue samples using TARP-4 multi-tumor tissue microarray. *Virchows Arch* 443: 122-132, 2003.

Downloaded from journals.physiology.org/journal/ajpcell at Univ of Szeged (160.114.150.232) on September 16, 2021.

14. **Fong P**. CFTR-SLC26 transporter interactions in epithelia. *Biophys Rev* 4: 107-116, 2012.

15. **Weintraub WH, and Machen TE**. pH regulation in hepatoma cells: roles for Na-H exchange, Cl-HCO3 exchange, and Na-HCO3 cotransport. *The American journal of physiology* 257: G317-327, 1989.

16. **Slepkov ER, Rainey JK, Sykes BD, and Fliegel L**. Structural and functional analysis of the Na+/H+ exchanger. *Biochem J* 401: 623-633, 2007.

17. **Pallagi-Kunstar E, Farkas K, Maleth J, Rakonczay Z, Jr., Nagy F, Molnar T, Szepes Z, Venglovecz V, Lonovics J, Razga Z, Wittmann T, and Hegyi P**. Bile acids inhibit Na(+)/H(+) exchanger and Cl(-)/HCO(3)(-) exchanger activities via cellular energy breakdown and Ca(2)(+) overload in human colonic crypts. *Pflugers Arch* 467: 1277-1290, 2015.

18. **Venglovecz V, Hegyi P, Rakonczay Z, Jr., Tiszlavicz L, Nardi A, Grunnet M, and Gray MA**. Pathophysiological relevance of apical large-conductance Ca(2)+-activated potassium channels in pancreatic duct epithelial cells. *Gut* 60: 361-369, 2011.

19. **Tobey NA, Koves G, and Orlando RC**. Human esophageal epithelial cells possess an Na+/H+ exchanger for H+ extrusion. *Am J Gastroenterol* 93: 2075-2081, 1998.

20. **Tobey NA, Reddy SP, Keku TO, Cragoe EJ, Jr., and Orlando RC**. Studies of pHi in rabbit esophageal basal and squamous epithelial cells in culture. *Gastroenterology* 103: 830-839, 1992.

21. **Shallat S, Schmidt L, Reaka A, Rao D, Chang EB, Rao MC, Ramaswamy K, and Layden TJ**. NHE-1 isoform of the Na+/H+ antiport is expressed in the rat and rabbit esophagus. *Gastroenterology* 109: 1421-1428, 1995.

22. **Ariyoshi Y, Shiozaki A, Ichikawa D, Shimizu H, Kosuga T, Konishi H, Komatsu S, Fujiwara H, Okamoto K, Kishimoto M, Marunaka Y, and Otsuji E**. Na+/H+

Downloaded from journals.physiology.org/journal/ajpcell at Univ of Szeged (160.114.150.232) on September 16, 2021.

678 exchanger 1 has tumor suppressive activity and prognostic value in esophageal squamous cell
679 carcinoma. *Oncotarget* 8: 2209-2223, 2017.
680 23. **Guan B, Hoque A, and Xu X**. Amiloride and guggulsterone suppression of
681 esophageal cancer cell growth in vitro and in nude mouse xenografts. *Front Biol (Beijing)* 9:
682 75-81, 2014.
683 24. **Yang SC, Chen CL, Yi CH, Liu TT, and Shieh KR**. Changes in Gene Expression
684 Patterns of Circadian-Clock, Transient Receptor Potential Vanilloid-1 and Nerve Growth
685 Factor in Inflamed Human Esophagus. *Sci Rep* 5: 13602, 2015.
686 25. **Zeng C, Vanoni S, Wu D, Caldwell JM, Wheeler JC, Arora K, Noah TK,**
687 **Waggoner L, Besse JA, Yamani AN, Uddin J, Rochman M, Wen T, Chehade M, Collins**
688 **MH, Mukkada VA, Putnam PE, Naren AP, Rothenberg ME, and Hogan SP**. Solute
689 carrier family 9, subfamily A, member 3 (SLC9A3)/sodium-hydrogen exchanger member 3
690 (NHE3) dysregulation and dilated intercellular spaces in patients with eosinophilic
691 esophagitis. *J Allergy Clin Immunol* 142: 1843-1855, 2018.
692 26. **Abdulnour-Nakhoul S, Nakhoul HN, Kalliny MI, Gyftopoulos A, Rabon E,**
693 **Doetjes R, Brown K, and Nakhoul NL**. Ion transport mechanisms linked to bicarbonate
694 secretion in the esophageal submucosal glands. *Am J Physiol Regul Integr Comp Physiol* 301:
695 R83-96, 2011.
696 27. **Abdulnour-Nakhoul S, Nakhoul NL, Wheeler SA, Wang P, Swenson ER, and**
697 **Orlando RC**. HCO3- secretion in the esophageal submucosal glands. *Am J Physiol*
698 *Gastrointest Liver Physiol* 288: G736-744, 2005.
699 28. **Tobey NA, Reddy SP, Khalbuss WE, Silvers SM, Cragoe EJ, Jr., and Orlando**
700 **RC**. Na(+)-dependent and -independent Cl-/HCO3- exchangers in cultured rabbit esophageal
701 epithelial cells. *Gastroenterology* 104: 185-195, 1993.

Downloaded from journals.physiology.org/journal/ajpcell at Univ of Szeged (160.114.150.232) on September 16, 2021.

29. **Wang J, Wang W, Wang H, and Tuo B**. Physiological and Pathological Functions of SLC26A6. *Front Med (Lausanne)* 7: 618256, 2020.

30. **Ko SB, Zeng W, Dorwart MR, Luo X, Kim KH, Millen L, Goto H, Naruse S, Soyombo A, Thomas PJ, and Muallem S**. Gating of CFTR by the STAS domain of SLC26 transporters. *Nat Cell Biol* 6: 343-350, 2004.

31. **Stewart AK, Yamamoto A, Nakakuki M, Kondo T, Alper SL, and Ishiguro H**. Functional coupling of apical Cl-/HCO3- exchange with CFTR in stimulated HCO3- secretion by guinea pig interlobular pancreatic duct. *Am J Physiol Gastrointest Liver Physiol* 296: G1307-1317, 2009.

32. **Saint-Criq V, and Gray MA**. Role of CFTR in epithelial physiology. *Cell Mol Life Sci* 74: 93-115, 2017.

33. **Kruger L, Pridgen TA, Taylor ER, Garman KS, and Blikslager AT**. Lubiprostone protects esophageal mucosa from acid injury in porcine esophagus. *Am J Physiol Gastrointest Liver Physiol* 318: G613-G623, 2020.

34. **Ao M, Venkatasubramanian J, Boonkaewwan C, Ganesan N, Syed A, Benya RV, and Rao MC**. Lubiprostone activates Cl- secretion via cAMP signaling and increases membrane CFTR in the human colon carcinoma cell line, T84. *Dig Dis Sci* 56: 339-351, 2011.

35. **Norimatsu Y, Moran AR, and MacDonald KD**. Lubiprostone activates CFTR, but not ClC-2, via the prostaglandin receptor (EP(4)). *Biochem Biophys Res Commun* 426: 374-379, 2012.

36. **Gharahkhani P, Fitzgerald RC, Vaughan TL, Palles C, Gockel I, Tomlinson I, Buas MF, May A, Gerges C, Anders M, Becker J, Kreuser N, Noder T, Venerito M, Veits L, Schmidt T, Manner H, Schmidt C, Hess T, Bohmer AC, Izbicki JR, Holscher AH, Lang H, Lorenz D, Schumacher B, Hackelsberger A, Mayershofer R, Pech O,**

Downloaded from journals.physiology.org/journal/ajpcell at Univ of Szeged (160.114.150.232) on September 16, 2021.

727 **Vashist Y, Ott K, Vieth M, Weismuller J, Nothen MM, Barrett's, Esophageal**
728 **Adenocarcinoma C, Esophageal Adenocarcinoma GenEtics C, Wellcome Trust Case**
729 **Control C, Attwood S, Barr H, Chegwidden L, de Caestecker J, Harrison R, Love SB,**
730 **MacDonald D, Moayyedi P, Prenen H, Watson RGP, Iyer PG, Anderson LA, Bernstein**
731 **L, Chow WH, Hardie LJ, Lagergren J, Liu G, Risch HA, Wu AH, Ye W, Bird NC,**
732 **Shaheen NJ, Gammon MD, Corley DA, Caldas C, Moebus S, Knapp M, Peters WHM,**
733 **Neuhaus H, Rosch T, Ell C, MacGregor S, Pharoah P, Whiteman DC, Jankowski J, and**
734 **Schumacher J**. Genome-wide association studies in oesophageal adenocarcinoma and
735 Barrett's oesophagus: a large-scale meta-analysis. *Lancet Oncol* 17: 1363-1373, 2016.
736 37. **Hassall E, Israel DM, Davidson AG, and Wong LT**. Barrett's esophagus in children
737 with cystic fibrosis: not a coincidental association. *Am J Gastroenterol* 88: 1934-1938, 1993.
738 38. **Holt EW, Yimam KK, and Liberman MS**. Esophageal adenocarcinoma in a 40-
739 year-old man with cystic fibrosis: coincidence or not? *Ochsner J* 13: 252-255, 2013.
740 39. **Li W, Wang C, Peng X, Zhang H, Huang H, and Liu H**. CFTR inhibits the invasion
741 and growth of esophageal cancer cells by inhibiting the expression of NF-kappaB. *Cell Biol*
742 *Int* 42: 1680-1687, 2018.
743 40. **Matsumoto Y, Shiozaki A, Kosuga T, Kudou M, Shimizu H, Arita T, Konishi H,**
744 **Komatsu S, Kubota T, Fujiwara H, Okamoto K, Kishimoto M, Konishi E, and Otsuji E**.
745 Expression and Role of CFTR in Human Esophageal Squamous Cell Carcinoma. *Ann Surg*
746 *Oncol* 2021.
747 41. **Vanoni S, Zeng C, Marella S, Uddin J, Wu D, Arora K, Ptaschinski C, Que J,**
748 **Noah T, Waggoner L, Barski A, Kartashov A, Rochman M, Wen T, Martin L, Spence J,**
749 **Collins M, Mukkada V, Putnam P, Naren A, Chehade M, Rothenberg ME, and Hogan**
750 **SP**. Identification of anoctamin 1 (ANO1) as a key driver of esophageal epithelial
751 proliferation in eosinophilic esophagitis. *J Allergy Clin Immunol* 145: 239-254 e232, 2020.

Downloaded from journals.physiology.org/journal/ajpcell at Univ of Szeged (160.114.150.232) on September 16, 2021.

Downloaded from journals.physiology.org/journal/ajpcell at Univ of Szeged (160.114.150.232) on September 16, 2021.

Figure 1

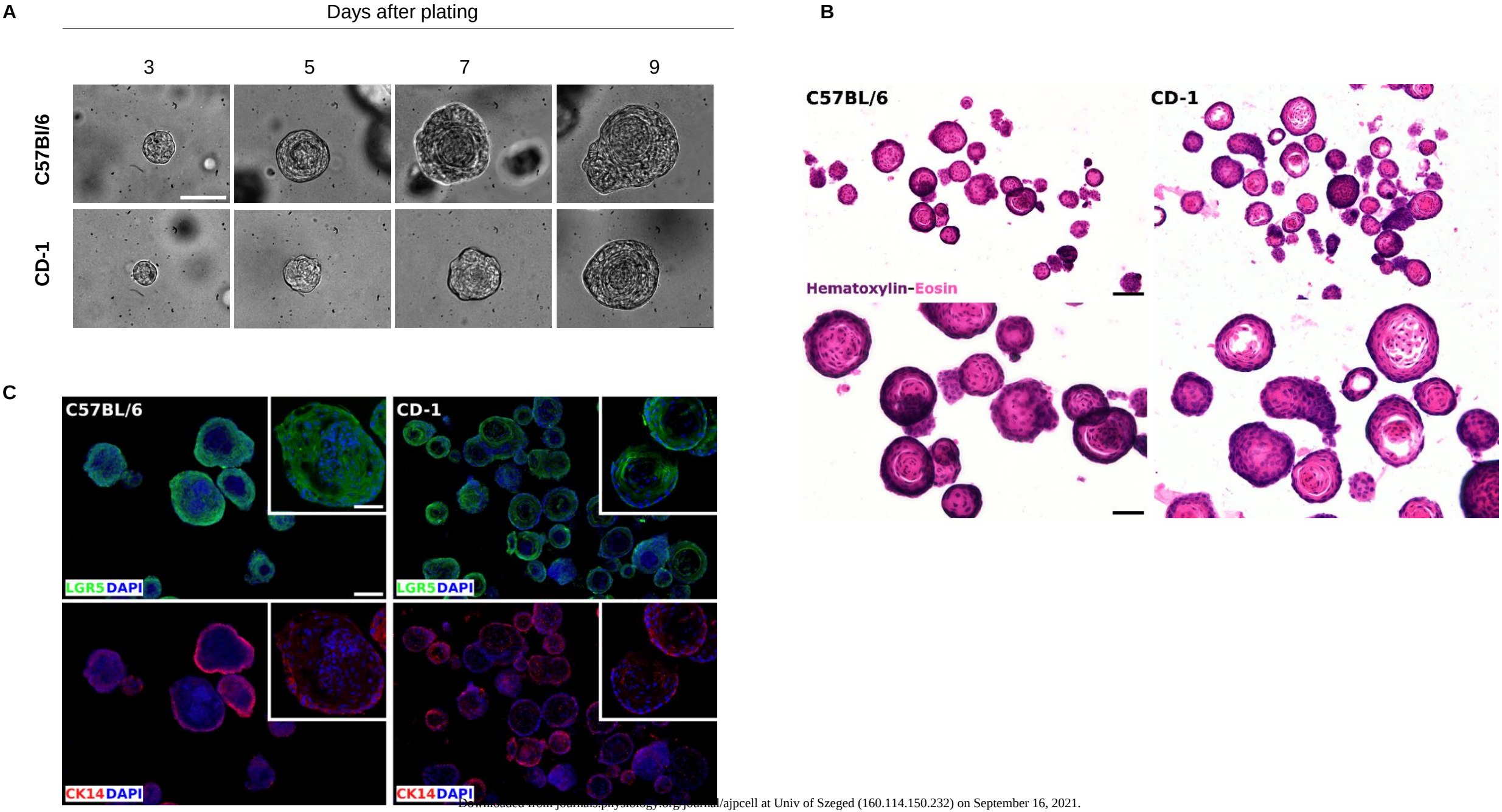

Downloaded from journals.physiology.org/journal/ajpcell at Univ of Szeged (160.114.150.232) on September 16, 2021.

Figure 2

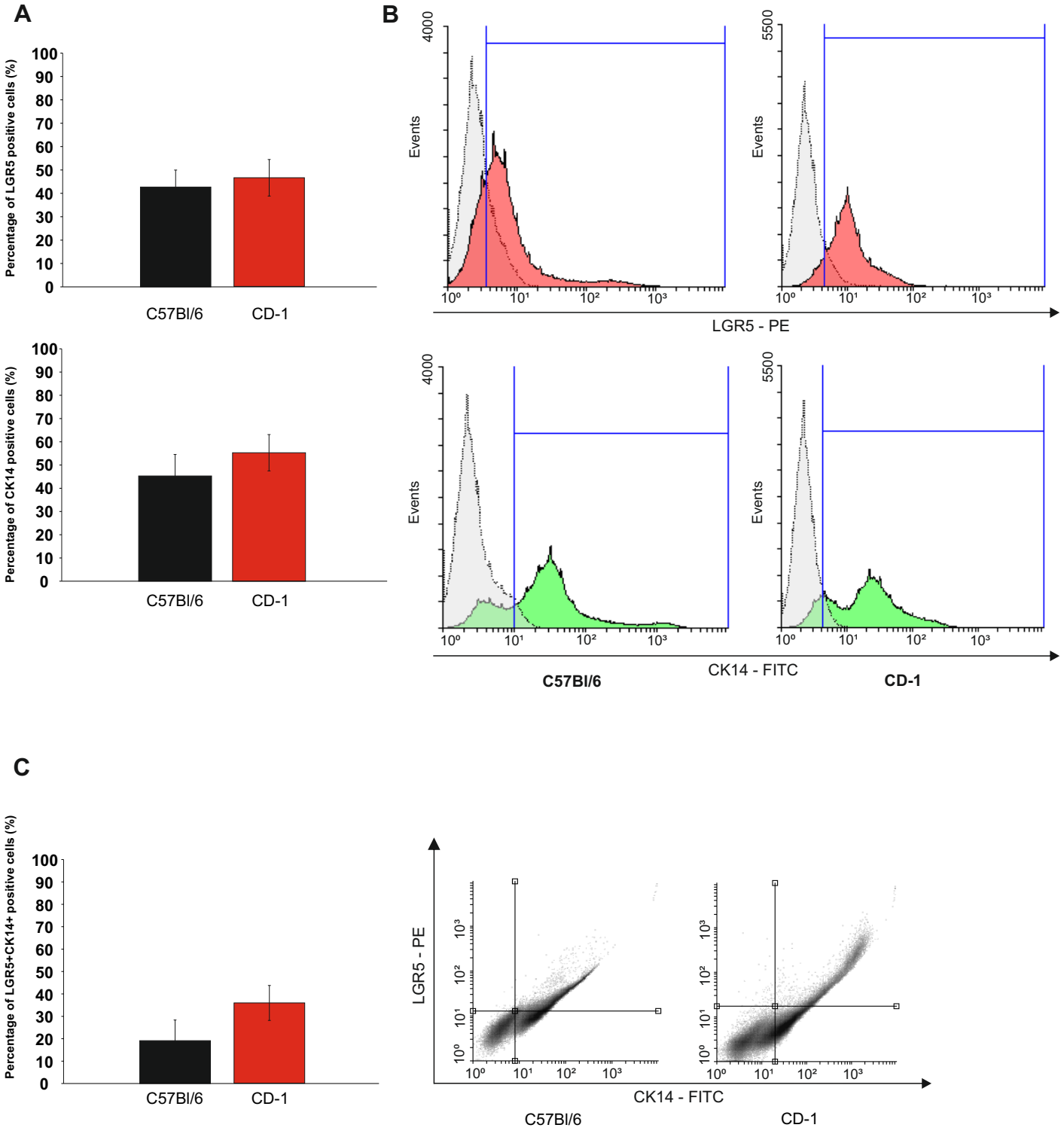

Downloaded from journals.physiology.org/journal/ajpcell at Univ of Szeged (160.114.150.232) on September 16, 2021.

Figure 3

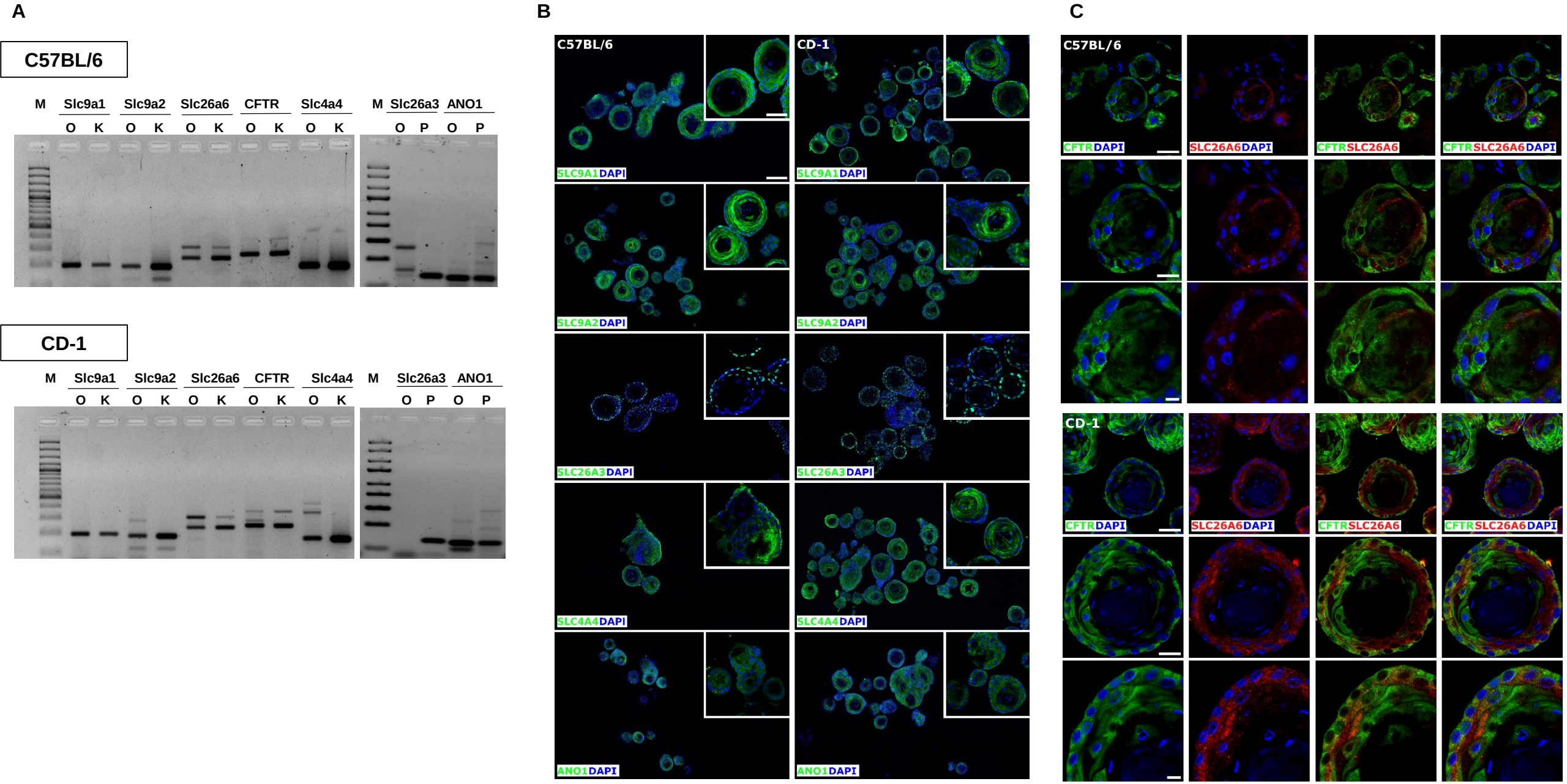

Downloaded from journals.physiology.org/journal/ajpcell at Univ of Szeged (160.114.150.232) on September 16, 2021.

Figure 4

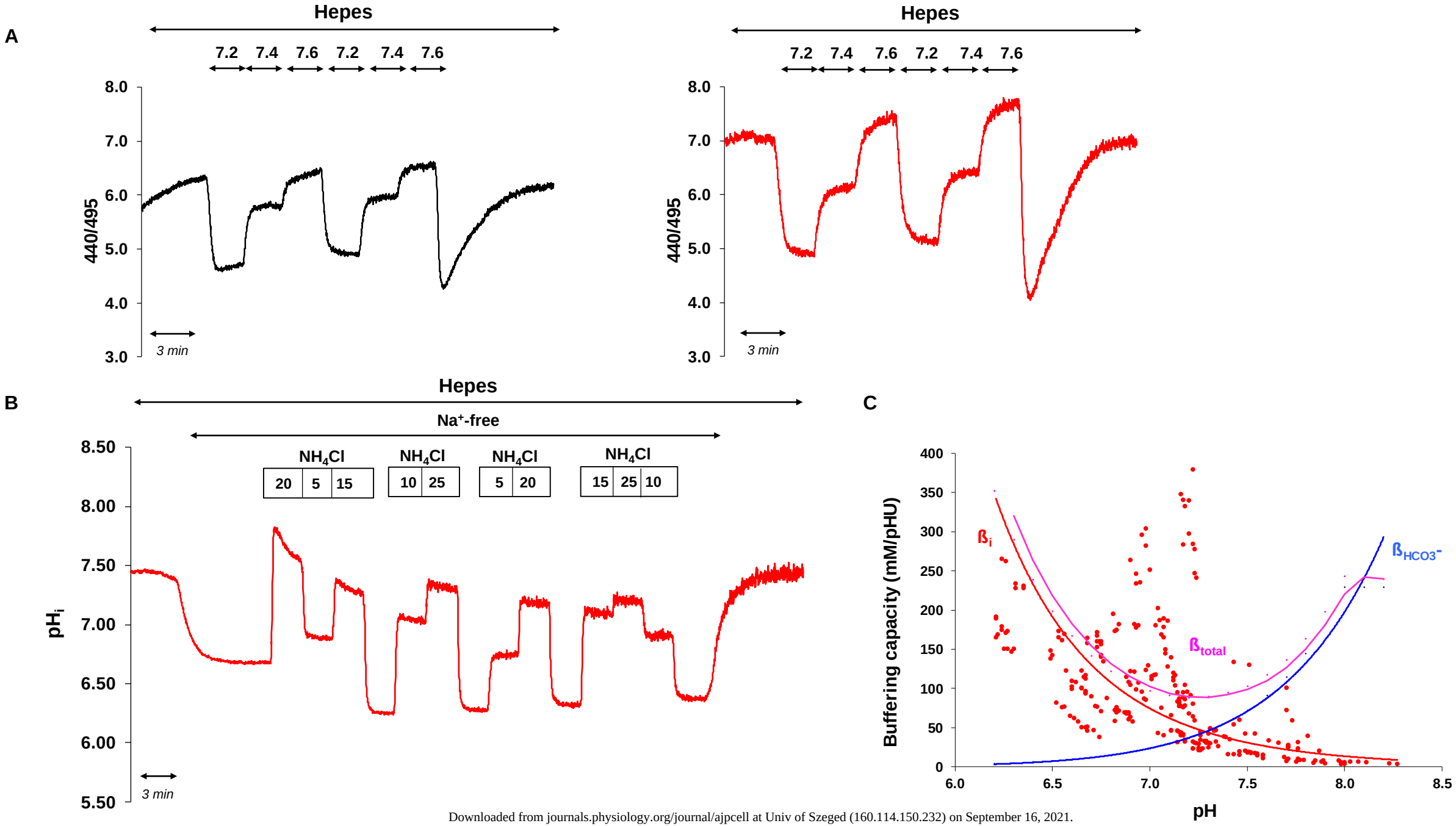

Downloaded from journals.physiology.org/journal/ajpcell at Univ of Szeged (160.114.150.232) on September 16, 2021.

Figure 5

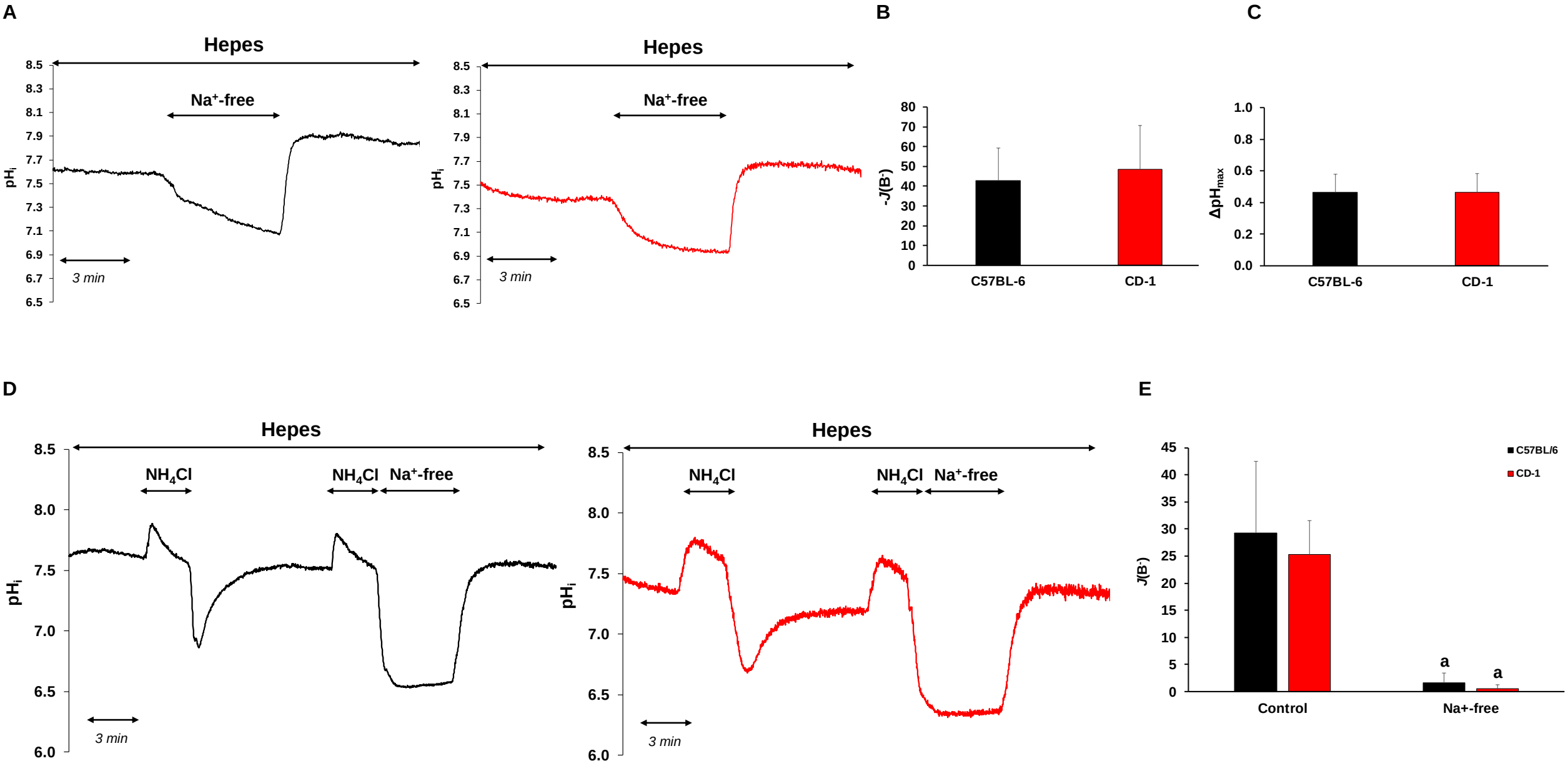

Downloaded from journals.physiology.org/journal/ajpcell at Univ of Szeged (160.114.150.232) on September 16, 2021.

Figure 6

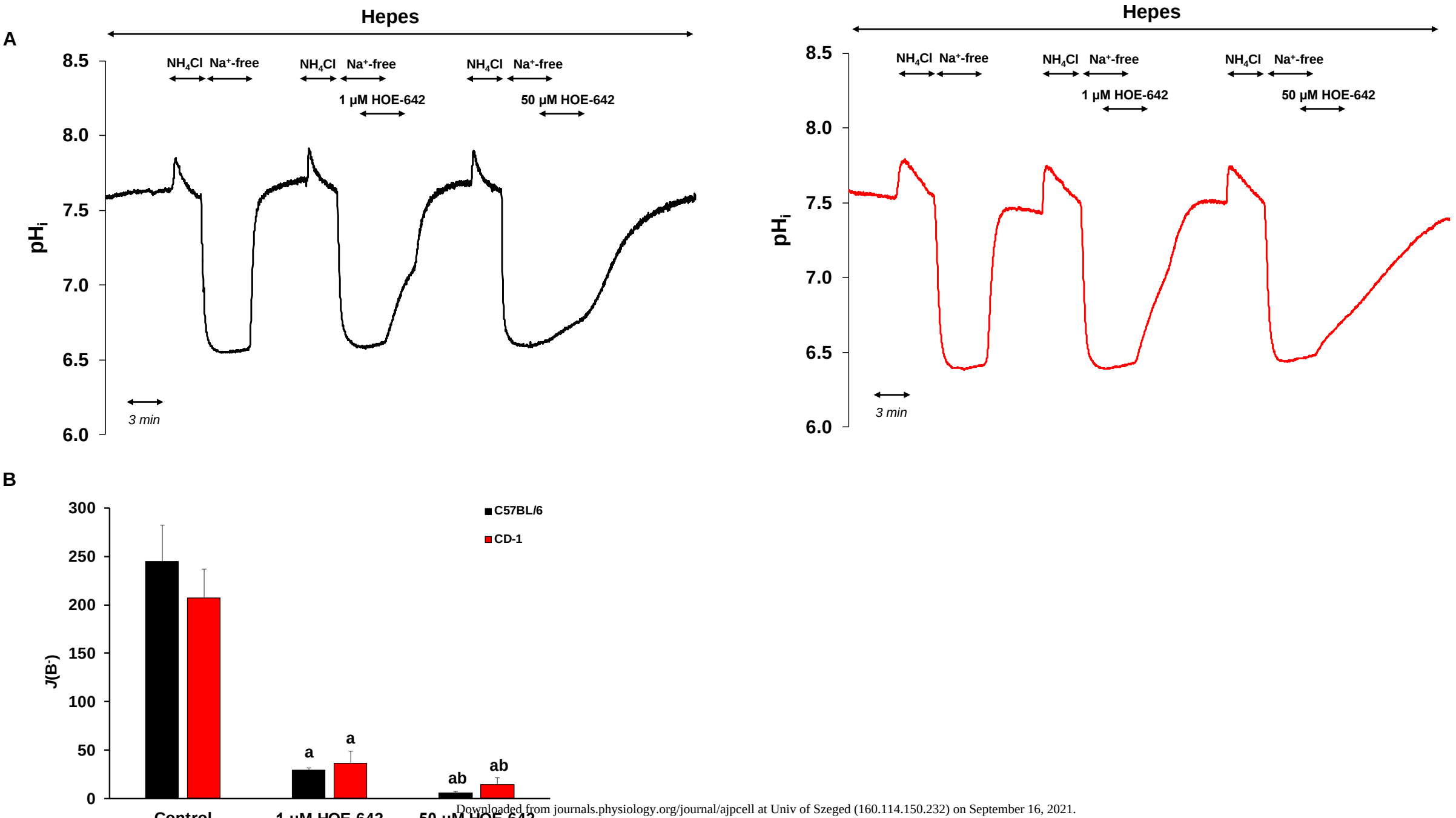

Downloaded from journals.physiology.org/journal/ajpcell at Univ of Szeged (160.114.150.232) on September 16, 2021.

Figure 7

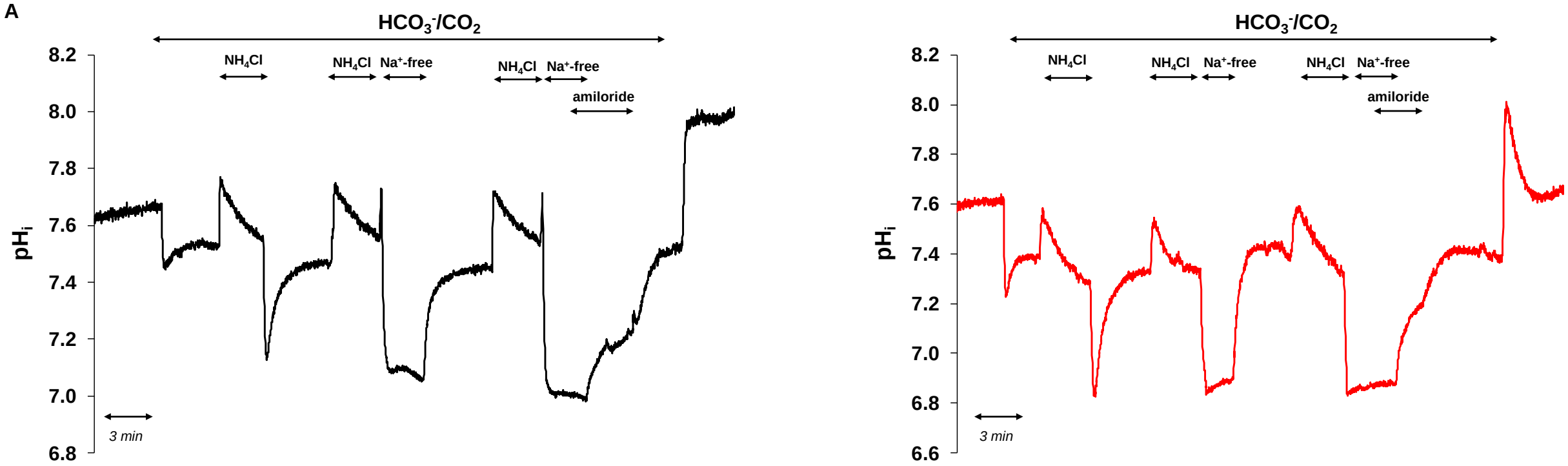

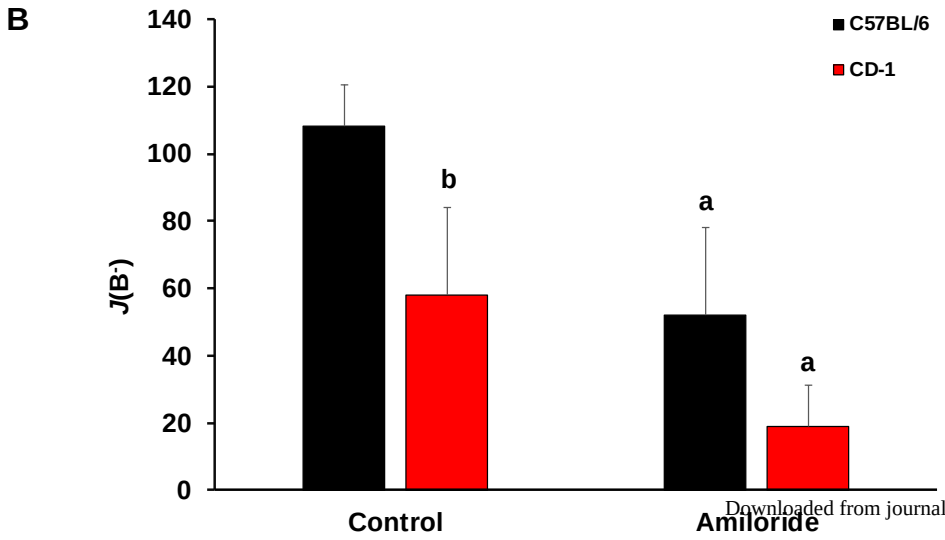

Downloaded from journals.physiology.org/journal/ajpcell at Univ of Szeged (160.114.150.232) on September 16, 2021.

Figure 8

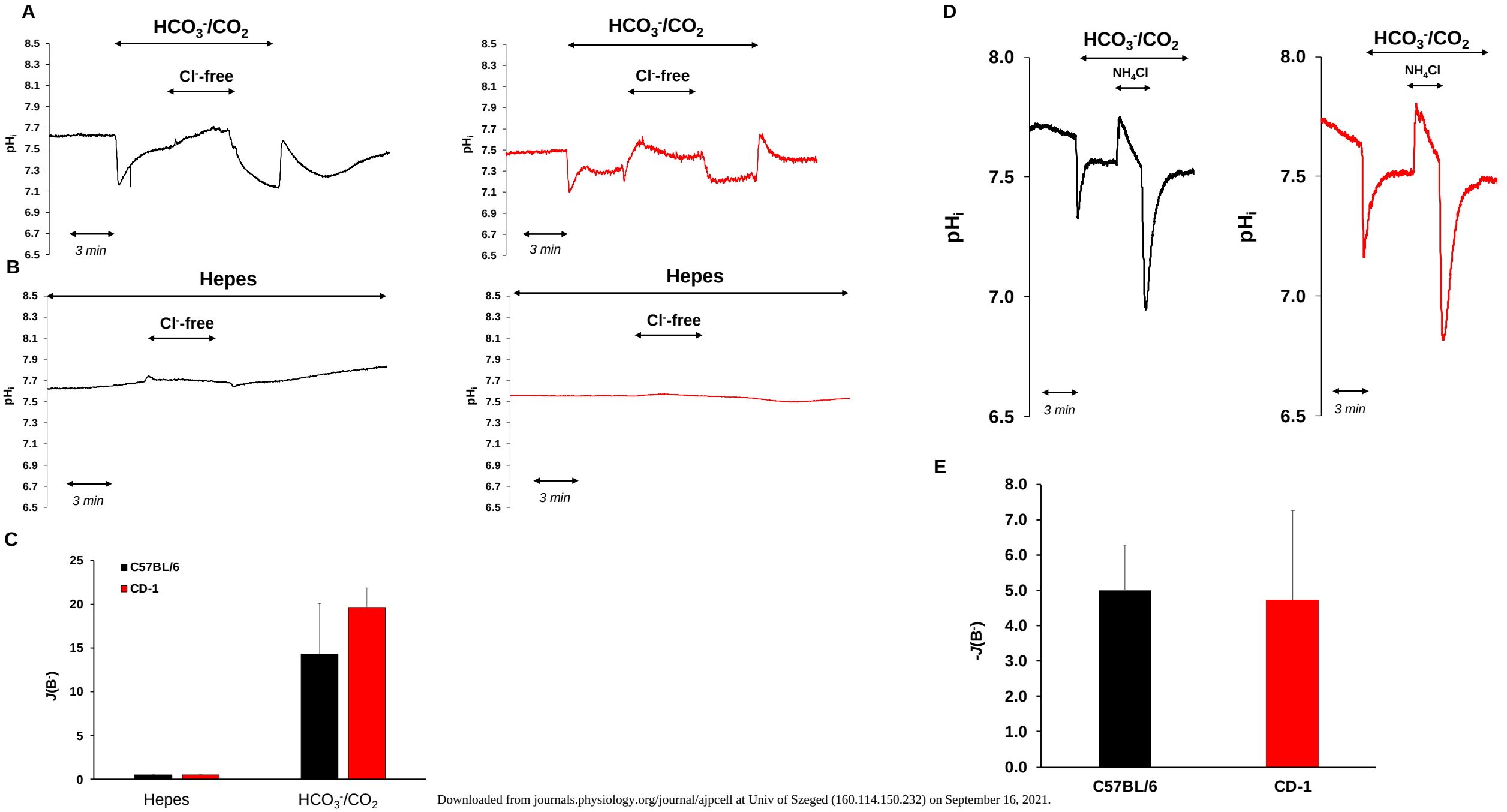

Downloaded from journals.physiology.org/journal/ajpcell at Univ of Szeged (160.114.150.232) on September 16, 2021.

Figure 9

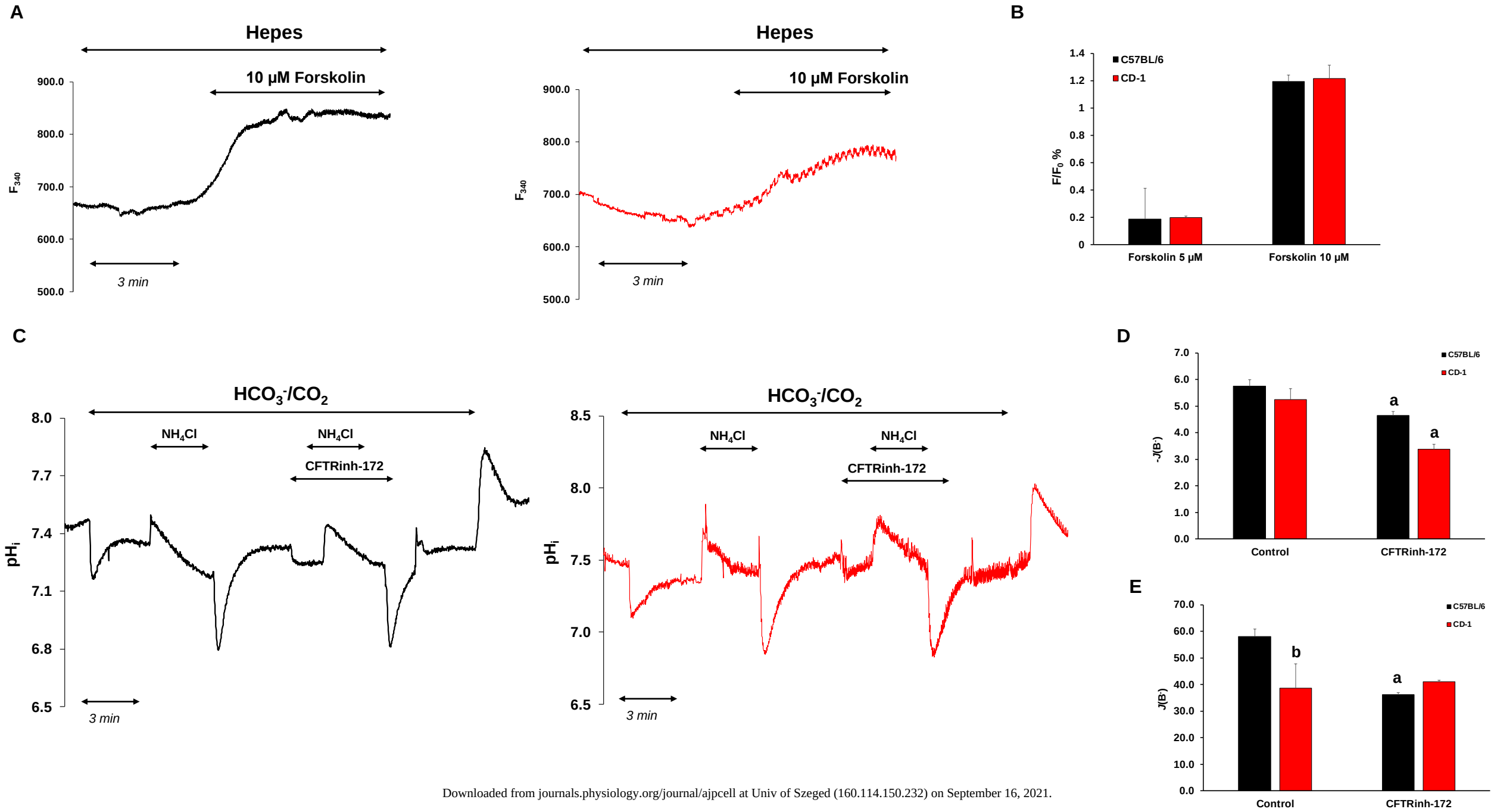

Downloaded from journals.physiology.org/journal/ajpcell at Univ of Szeged (160.114.150.232) on September 16, 2021.

Figure 10

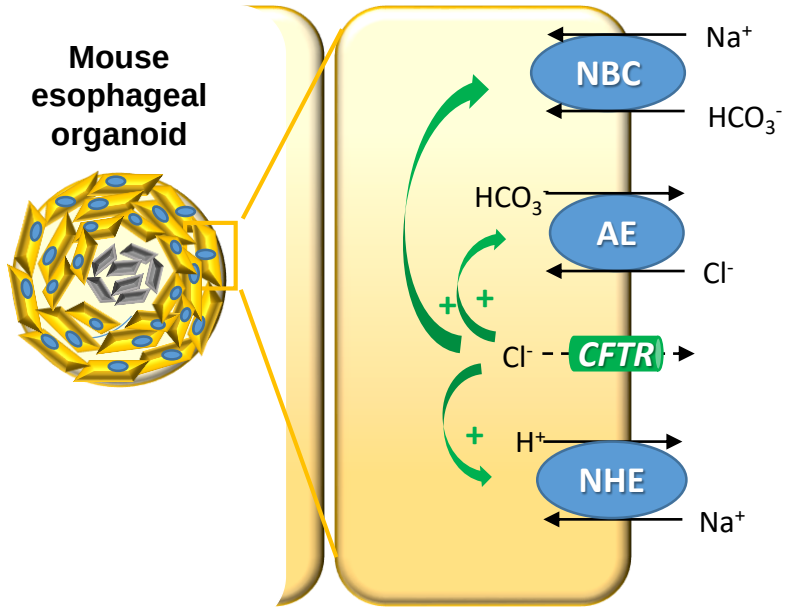

Downloaded from journals.physiology.org/journal/ajpcell at Univ of Szeged (160.114.150.232) on September 16, 2021.

	Standard HEPES	Standard HCO_3^-	NH_4Cl HEPES	High-K^+ HEPES	NH_4Cl HCO_3^-	Na^+-free HEPES	Na^+-free HCO_3^-	Cl^--free HEPES	Cl^--free HCO_3^-
NaCl	140	115	110	5	95				
KCl	5	5	5	130	5	5	5		
$MgCl_2$	1	1	1	1	1	1	1		
$CaCl_2$	1	1	1	1	1	1	1		
HEPES acid	10		10			10		10	
Glucose	10	10	10	10	10	10	10	10	10
$NaHCO_3$		25			25				25
NH_4Cl			20		20				
Na-HEPES				10					
NMDG-Cl						140	115		
Na-gluconate								140	115
Mg-gluconate								1	1
Ca-gluconate								6	6
K_2-sulfate								2.5	2.5
Choline HCO_3^-							25		
Atropine							0.01		

Table 1

Downloaded from journals.physiology.org/journal/ajpcell at Univ of Szeged (160.114.150.232) on September 16, 2021.

Primary antibodies	Company	Cat. No.	Dilution
Slc9a1	Alomone	ANX-010	1:100
Slc9a2	Alomone	ANX-002	1:100
Slc26a3	Invitrogen	PA5-68530	1:600
Slc26a6	Santa Cruz Biotechnology	sc-515230	1:200
Slc4a4	Abcam	ab187511	1:100
CFTR	Alomone	ACL-006	1:200
ANO1	Alomone	ACL-011	1:200

Table 2

Downloaded from journals.physiology.org/journal/ajpcell at Univ of Szeged (160.114.150.232) on September 16, 2021.

Gene	Reverse primer	Forward primer	Product size (bp)
Slc9a1	TGGCTCTACTGTCCTTTGGG	GAGGAGGAAGATGAGGACGG	194
Slc9a2	GAAATCAGGCTGCCGAAGAG	CTACTTCATGCCAACTCGCC	183
Slc26a3	ACCCTTTGAGATGGTCCAGG	TTCCTTCCCACTAGCCACTG	161
Slc26a6	AGCTCCTGGTTACTGTCCAC	TCATTGGGGCCACTGGTATT	235
Slc4a4	CAGCCACATACCAGGGAAGA	CGGCTTTGCTAGTCACCATC	171
CFTR	TCTGCATGGGTTCTGGGAAT	GAGCAATGTCTGGCAGTACG	249
ANO1	GGGGCTGTGGTTGTTACAAG	ATCCCCAAAGACATCAGCCA	150

Table 3

Downloaded from journals.physiology.org/journal/ajpcell at Univ of Szeged (160.114.150.232) on September 16, 2021.